

FLAPPING-WING THRUST IN COMPRESSIBLE FLOW

Wolfgang Send

Institute of Aeroelasticity, German Aerospace Center (DLR)
Göttingen, Germany

Keywords: *Compressible Flow, Unsteady Aerodynamics, Aerodynamic Power*

Abstract

The phenomenon of thrust generation by a coupled bending and torsional motion is surveyed ranging from incompressible flow to the transonic region. 2D wing sections and 3D planforms are studied. The paper also touches on the question, whether flapping-wing thrust for larger airplanes is physically possible.

1 Introduction

While in nature the flapping wing is the exclusive means for thrust generation which has been optimised in the course of the evolution, its application in aeronautics has not yet succeeded even after more than one hundred years of powered flight. The author has initiated a research programme *Advanced Adaptive Airplane Technologies (A³T)*, a part of which coincides within the DLR project *HighPerFLEX (High-Performance Flexible Aircraft)* lasting from 2004 to 2006. The incidentally observed increase in speed of a transport aircraft during a flutter test due to its oscillating wings gave the cause for the present investigation. The oscillations were induced by an exciter at the wing tip.

Do exist benefits from forced oscillation of wings to technical use? The research may be seen within the scope of the fast growing field of interest *Adaptive Wings*. Fig. 1 shows the aerodynamic power coefficients of a coupled pitching and plunging motion for a 2D flat plate in incompressible flow.

The figure displays the basic mechanism of flapping-wing propulsion for a gliding airplane or animal: The power of a strong bending (plunging in 2D) motion is converted into thrust with aid of a torsional (pitching in 2D) motion. The highest propulsive efficiency is achieved for an active pitch, which, however, requires hardly any power. The details of the contour plots are explained in the course of the paper.

These contour plots are based on the historic analytical solution developed by Küssner [1] and Theodorsen [2]. At the same time Garrick [3] published his paper on the propulsive mechanism. The very first solution by a series expansion dates back to Birnbaum's explanation of the flutter problem [4], which simply is the inverse mechanism.

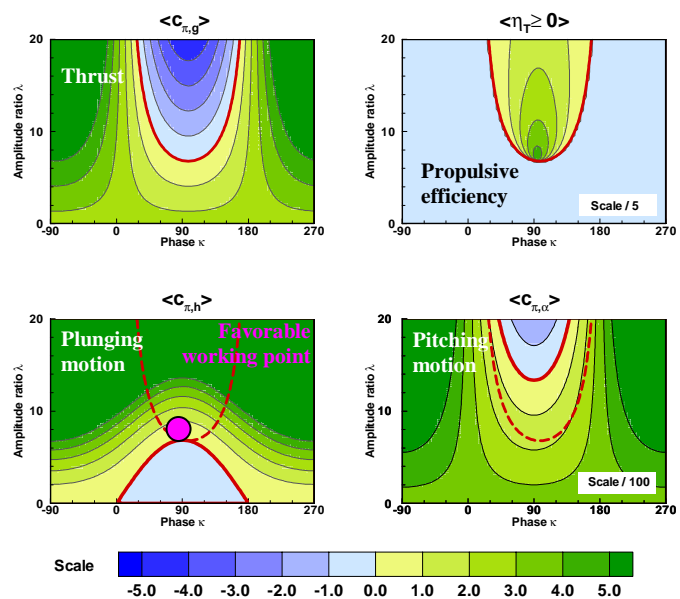


Fig. 1. Mechanism of propulsion, 2D thin plate.
 $Ma = 0, \omega^* = 0.15, x_p / c = 0.25.$

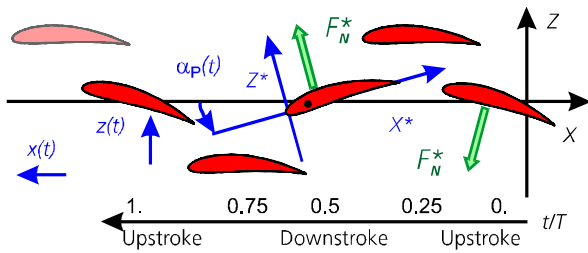


Fig. 2. 2D Kinematics and normal force F_N^* .

Unfortunately, all of these papers favor the more powerful, but less efficient mode of phase shift for the plunging versus the pitching motion, in which the leading edge sweeps over the largest possible frontal area. This type of motion maximizes the ‘suction effect’, which also occurs in the limiting case of a pure plunging motion. Though this suction force theoretically is present and also has been identified in some experiments, its source needs carefully to be located and discussed [10]. The contour plots in Fig. 1 omit the contribution by the leading edge suction. The data rest on the normal force distribution from the pressure along the chord.

Animal flight makes use of the opposite mode: Small angles of incidence turn the force appearing normal to the plunging chord slightly towards the direction of the animal’s trajectory as shown in Fig. 2. With a positive pitch angle during the upstroke the negative normal force decomposes into a forward component, which gives the thrust, and the lift component perpendicular to the flow, against which work has to be done. During the downstroke the wing experiences a positive normal force, which again, with aid of a now negative pitch angle, results in a thrust component. The work done is converted into thrust with a high efficiency.

In Fig. 1 a specific aspect has to be pointed out. The contour plots show that the generation of thrust with a flapping wing is possible with driving the plunging motion only. A sufficiently flexible wing will start pitching automatically, because it is aerodynamically excited. Self-excitation for the pitch motion (the blue area in the lower right contour plot) occurs in the range of an efficiency less than about 0.4. The range of high efficiency requires a small input of power for the pitching motion also. To the

author’s knowledge, none of the many existing models for flapping flight around the world is optimized regarding this essential effect. In former times, the realization might have been a serious mechanical problem. The progress in adaptive techniques has made feasible the active control of the pitching motion.

Among the numerous papers focusing on flapping-wing thrust the admirable work of DeLaurier needs to be mentioned, who developed the first full-scale piloted ornithopter [5]. In one of his early papers on flapping flight he mentions the average propulsive efficiency of the flying robot pterosaur, built by the National Air and Space Museum in Washington DC in the mid 1980s. The best value for efficiency is around 0.4 [6] and exemplifies the problem of active pitch control. Platzer and Jones [7] have investigated the both effects of thrust production and power extraction of the coupled flapping and pitching motion theoretically and in a series of experiments [8].

The following investigation concentrates on motion parameters which are typical of the animal-flight conditions as just discussed.

2 Nomenclature and Notation

α_{0H}	Amplitude of $\dot{z}(t)/\dot{x}(t)$ for small angle
α_0	Amplitude pitch [-]
h_0	Amplitude plunge [m]
λ, λ_c	Amplitude ratio = $\frac{h_0}{\alpha_0 \cdot c/2}$, $\lambda_c = \lambda/2$
x_L	Centre of steady pressure distribution
c	Chord length [m]
ω	Circular frequency = $2\pi f$ [1/s]
\mathbf{x}	Coordinate vector = (x, y, z)
X	Degree of freedom (DOF) $\{g, h, \alpha\}$
ρ	Density of the fluid [kg/m ³]
a_X	Dimensionless amplitude of DOF X $a_h = h_0/(c/2)$, $a_\alpha = \alpha_0$
$D(t)$	Drag force [N]
q_0	Dynamic pressure = $\frac{1}{2} \cdot \rho \cdot u_0^2$ [N/m ²]
F_0	Force constant = $q_0 \cdot S$

$F_N^*(t)$	Force normal to the wing planform [N]
f	Frequency [Hz] of periodic motion
u_0	Kinematic x-velocity [m/s]
$L(t)$	Lift force [N]
Ma	Mach number = u_0/c_s [-]
$c_{M,X}(t)$	Moment coefficient of DOF X = $M_X(t)/(F_0 \cdot c \cdot a_X)$
$g(t)$	Motion, gliding = $u_0 \cdot t$ [m]
$x(t)$	Motion in x-direction = $-g(t)$ [m]
$z(t)$	Motion in z-direction = $-h(t)$ [m]
$\alpha_H(t)$	Motion, apparent inflow angle [-]
$\alpha_P(t)$	Motion, pitch = $\alpha_S + \alpha_0 \cos \omega t$ [-]
$h(t)$	Motion, plunge = $h_0 \cos(\omega t + \kappa)$ [m]
$c_{N,X}(t)$	Normal force coefficient of DOF X = $F_{N,X}(t)/(F_0 \cdot a_X)$
T	Period of cyclic motion = $1/f$ [s]
κ	Phase shift of plunge versus pitch [-]
t	Physical time [s]
x_p	Pitch axis, absolute position
ξ_p	Pitch axis, relative position = x_p/c
S	Planform area of the wing
$P_X(t)$	Power at DOF X [W]
$c_{\Pi,X}(t)$	Power coefficient of DOF X = $P_X(t)/(F_0 \cdot u_0 \cdot \alpha_0^2)$
$\langle c_{\Pi,X} \rangle$	Power coefficient averaged over T
$c_p(x,t)$	Pressure coefficient = $(p(x,t) - p_0)/q_0$
p_0	Pressure, hydrostatic ~ [N/m ²]
$p(\mathbf{x},t)$	Pressure, local ~ in the fluid [N/m ²]
η_T	Propulsive efficiency $\frac{-\langle P_g \rangle}{\langle P_h \rangle + \langle P_\alpha \rangle}$
ω^*, ω_c^*	Reduced frequency $\frac{\omega \cdot c/2}{u_0}$, $\omega_c^* = 2\omega^*$
x, y, z	Space-fixed coordinates [m]
x^*, y^*, z^*	Body-fixed coordinates [m]
c_s	Speed of sound in the fluid [m/s]
α_S	Steady angle of incidence [-]

The notation of the motion follows the historic papers mentioned at the beginning. For $t = 0$ the pitch angle is maximum positive. Without any phase shift ($\kappa = 0^\circ$), the wing starts at the bottom in its lowest position. Fig. 2 shows a phase shift of $\kappa = 90^\circ$, for which the highest pitch angle and the largest plunge velocity during upstroke coincide. The same phase shift leads to the interesting features in the centre of each graph in Fig. 1.

For $P_X > 0$ power is consumed at DOF X. Power is required for supporting the motion.

For $P_X < 0$ power is released at DOF X. Power is gained by the motion and has to be consumed for maintaining the motion.

3 The Basic Mechanism in 2D Motion

The translational motion ($x(t), z(t)$) of the 2D wing section (profile) in Fig. 2 leads to the angle $\alpha_H(t)$ of the slope

$$\tan \alpha_H(t) = \frac{\dot{z}(t)}{\dot{x}(t)} = \frac{h_0 \cdot \omega \cdot \sin(\omega t + \kappa)}{-u_0}. \quad (1)$$

For small angles the tangent may be linearized by $\tan \alpha_H(t) \cong \alpha_H(t)$. With this assumption the amplitude of the angle of incidence due to the plunging motion can be expressed relatively to the pitch amplitude by the two coefficients λ and ω^* :

$$\frac{\alpha_{0H}}{\alpha_0} = \frac{h_0 \cdot \omega}{u_0 \cdot \alpha_0} = \lambda \cdot \omega^* = \lambda_c \cdot \omega_c^* \quad (2)$$

The fluid's effect on the profile is like it would be turned by the angle $\alpha_H(t)$. Moving in the fluid the profile experiences periodic normal forces due to the both motions pitch and plunge. While the normal force due to plunge does not turn the profile geometrically, the pitch so does.

The normal force in the body-fixed coordinate system (Fig. 2) can be estimated from the 2D lift formula for the inclined plate

$$F_N^*(t) \approx F_0 \cdot 2\pi\alpha(t), \quad \alpha(t) = \alpha_P(t) + \alpha_H(t). \quad (3)$$

The force in Eqn. (3) now is transformed into the reference system of the averaged translational motion, the direction of u_0 .

$$\mathbf{F} = \begin{bmatrix} D \\ 0 \\ L \end{bmatrix} = \begin{bmatrix} F_N^* \cdot \sin \alpha_p \\ 0 \\ F_N^* \cdot \cos \alpha_p \end{bmatrix} \equiv F_0 \cdot 2\pi \cdot \begin{bmatrix} \alpha_p^2 + \alpha_p \cdot \alpha_H \\ 0 \\ \alpha_p + \alpha_H \end{bmatrix} \quad (4)$$

For small pitch angles $\sin \alpha \cong \alpha$ and $\cos \alpha \cong 1$ are applied, which gives the well known result that an unsteady harmonic motion produces a harmonically varying lift force and a drag force with the double period. The term for the normal force will be replaced by the proper functions for unsteady motion in which the shedding vortices lead to delayed or advancing reactions of the forces relative to the kinematic motion (e.g. [9]).

The corresponding powers are given by *force times velocity*

$$P_{trans} = \mathbf{F} \cdot \mathbf{v}_{kin}, \quad \mathbf{v}_{kin} = -[\dot{x}, 0, \dot{z}] \quad (5)$$

and *moment times angular velocity*

$$P_{rot} = M_p(t) \cdot [-\dot{\alpha}_p(t)], \quad M_p(t) = F_N^*(t) \cdot (x_p - x_L). \quad (6)$$

The force \mathbf{F} in the preceding equations is the reaction force of the fluid on the moving body. Thus, the velocity in the formulas has to be the kinematic motion of the fluid relative to the body, which is the negative value of the body's velocity in the fluid. The fluid is at rest.

If the centre of the pressure distribution x_L is close to or even coincides with the centre of rotation x_p , the power due to rotation is negligible in the quasi-steady case.

The basic mechanism of thrust generation is understood after evaluating Eqn. (5). The translational power is split into the contributions from the DOFs g and h :

$$P_{trans} = P_g + P_h = -D \cdot \dot{x} - L \cdot \dot{z} \quad (7)$$

A straightforward calculation leads to $P_g(t)$ and $P_h(t)$. From the mean value during one cycle of motion

$$\langle P_x \rangle = \frac{1}{T} \int_0^T P_x(t) \cdot dt \quad (8)$$

the power coefficients are computed, given by

$$\langle c_{\Pi,x} \rangle = \frac{\langle P_x \rangle}{F_0 \cdot u_0 \cdot \alpha_0^2}. \quad (9)$$

The results for the translational motions are shown in Fig. 3 and read

$$\langle c_{\Pi,g} \rangle = -\pi \cdot [\omega^* \lambda \cdot \sin \kappa - 1], \quad (10)$$

$$\langle c_{\Pi,h} \rangle = +\pi \omega^* \lambda \cdot [\omega^* \lambda - \sin \kappa]. \quad (11)$$

For the favorable case $\kappa = 90^\circ$ thrust is gained for $\omega^* \lambda > 1$. From the definition in Eqn. (2) propulsion is effected by a large plunging motion for which the amplitude of the apparent inflow angle $\alpha_H(t)$ is larger than the amplitude of the geometric pitch angle $\alpha_p(t)$. The propulsive efficiency η_T is given by

$$\eta_T = \frac{-\langle c_{\Pi,g} \rangle}{\langle c_{\Pi,h} \rangle + \langle c_{\Pi,\alpha} \rangle}, \quad \langle c_{\Pi,g} \rangle < 0. \quad (12)$$

4 The Mechanism in 2D Subsonic Flow

The investigation in subsonic flow requires the normal force and moment coefficients to be extended into the domain of compressible flow. The following results rest on the solution of Possio's integral equation for the plunging and pitching thin plate for subsonic flow. The numerical work has been done by Carstens [11].

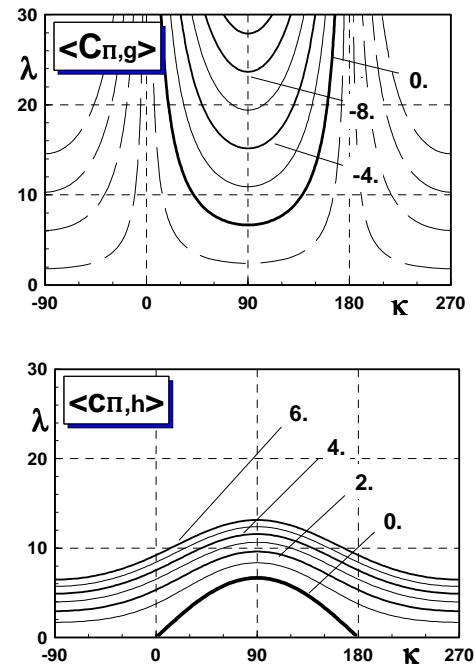


Fig. 3. The contours of Eqns. (10) and (11) for $\omega^* = 0.15$ (taken from [10]).

With kind permission of the author the set of solutions in Tab. 1 is available in the Internet as part of a flutter program for simple flutter analyses of the plunging and pitching plate [12].

Type Y ↓	Plunging	Pitching
Normal force	$c_{N,h}(Ma, \omega^*)$	$c_{N,\alpha}(Ma, \omega^*, \xi_P)$
Moment	$c_{M,h}(Ma, \omega^*, \xi_P)$	$c_{M,\alpha}(Ma, \omega^*, \xi_P)$

Tab. 1: Set of complex functions for computing the power coefficients.

The solutions are linear with respect to the amplitudes and the DOFs. They are represented by their magnitudes $\bar{c}_{Y,X}$ and phases $\phi_{Y,X}$. E.g., the normal force due to the pitching motion reads:

$$F_{N,\alpha}^*(t) = F_0 \cdot \bar{c}_{N,\alpha}(Ma, \omega^*, \xi_P) \cdot \cos(\omega t + \phi_{N,\alpha}) \cdot \alpha_0 \quad (13)$$

The phase $\phi_{N,\alpha}$ in Eqn. (13) depends on the same parameters as the magnitude $\bar{c}_{N,\alpha}$ does. The discussion of the basic mechanism in chapter 3 did not yet include the complete set of the 2D power coefficients for plunging and pitching motion. All power coefficients depend on the same set of parameters:

$$\langle c_{\Pi,X}(Ma, \omega^*, \xi_P, \lambda, \kappa) \rangle. \quad (14)$$

The functions are formed by superposition of the respective force and moment coefficients:

$$\langle c_{\Pi,g} \rangle = \frac{1}{2} \cos \alpha_S \bar{c}_{N,h} \cos(\phi_{N,h} + \kappa) + \bar{c}_{N,\alpha} \cos \phi_{N,\alpha} \quad (15)$$

$$\langle c_{\Pi,h} \rangle = \frac{1}{2} \omega^* \lambda \bar{c}_{N,h} \sin(\phi_{N,h} + \kappa) + \bar{c}_{N,\alpha} \sin(\phi_{N,\alpha} - \kappa) \quad (16)$$

$$\langle c_{\Pi,\alpha} \rangle = -\omega^* \lambda \bar{c}_{M,h} \sin(\phi_{M,h} + \kappa) + \bar{c}_{M,\alpha} \sin \phi_{M,\alpha} \quad (17)$$

The complete set of functions including an additional in-plane motion may be found in [9]. The preceding three equations reduce to Eqns. (10) and (11) for small reduced frequencies. Depending on the pitch axis, the power coefficient is small or vanishes.

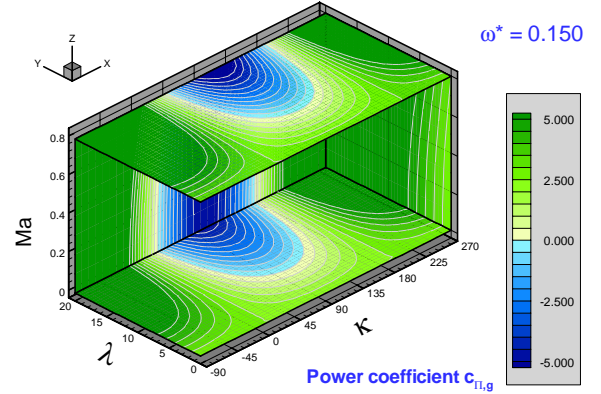


Fig. 4a: Subsonic flow $\langle c_{\Pi,g} \rangle$

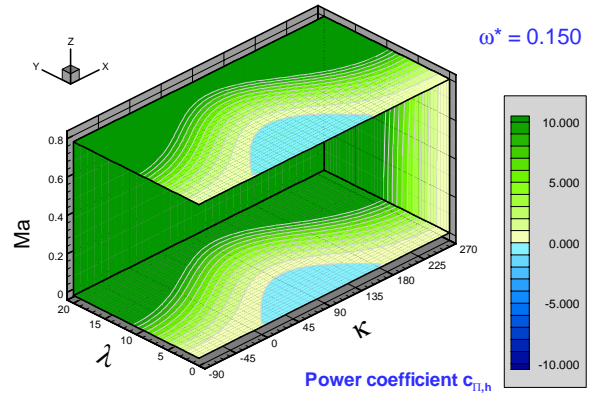


Fig. 4b: Subsonic flow $\langle c_{\Pi,h} \rangle$

The four plots in Fig. 4 show that the influence of the Mach number alters the contour lines in particular for $\langle c_{\Pi,\alpha} \rangle$. The influence approximately is the Prandtl-Glauert factor $1/\sqrt{1-Ma^2}$. Since the force and moment coefficients depend all the same way on the Mach number, the efficiency remains almost unchanged. The investigation has been carried for the parameters given in Tab. 2. The pitch axis is kept at quarter chord in all computations.

0.0	$\leq Ma \leq$	0.8	(16)
0.1	$\leq \omega^* \leq$	1.1	(40)
0.0	$\leq \lambda \leq$	20	(40)
-90	$\leq \kappa \leq$	270	(36)

Tab. 2: Set of parameters for database.

The full set of data may be found on the Internet page www.aniprop.de/icas06.

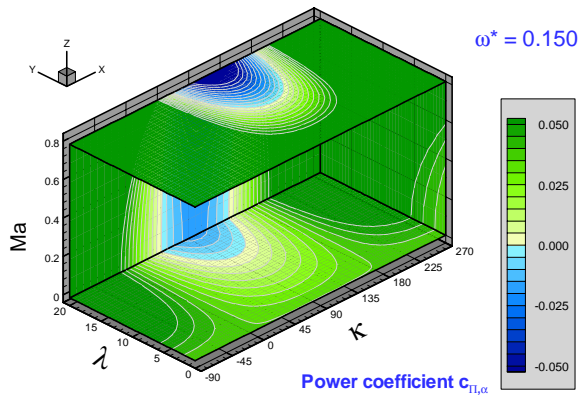


Fig. 4c: Subsonic flow $\langle c_{II,\alpha} \rangle$

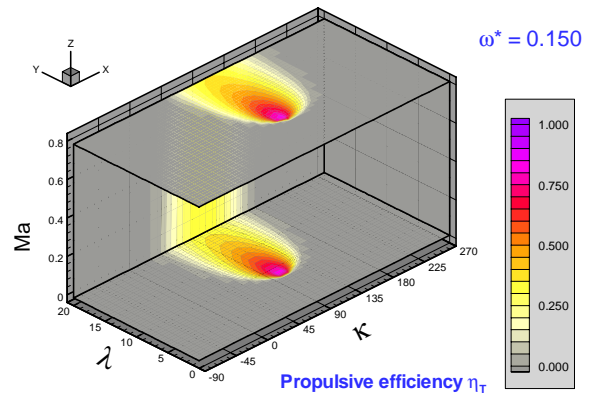


Fig. 4d: Subsonic flow η_T

5 Transonic 2D Euler Flow

The effects of the coupled pitching and plunging motion in transonic flow are investigated for selected profiles and parameters. The flow solver [13] is an upwind-scheme using the technique of flux-vector-splitting according to van Leer on a structured grid. In general, the numerical solution in a viscous and compressible fluid causes a steady drag which depends on two sources, the friction tangential to a surface element ΔS and the pressure normal

to it (see Fig. 6). Though the viscous effect tangential to the surface is not considered in an Euler solution, the pressure distribution implies numerical drag to an extent which depends on the particular computational scheme. The unsteady motion triggers the physical effect which has to be separated from the numerical one. As an example, the data for the solution shown in Fig. 5 are given in Tab. 4. The drag coefficient c_D for steady flow and the power coefficient for gliding are comparable terms. The flapping motion reduces the drag compared to steady flow.

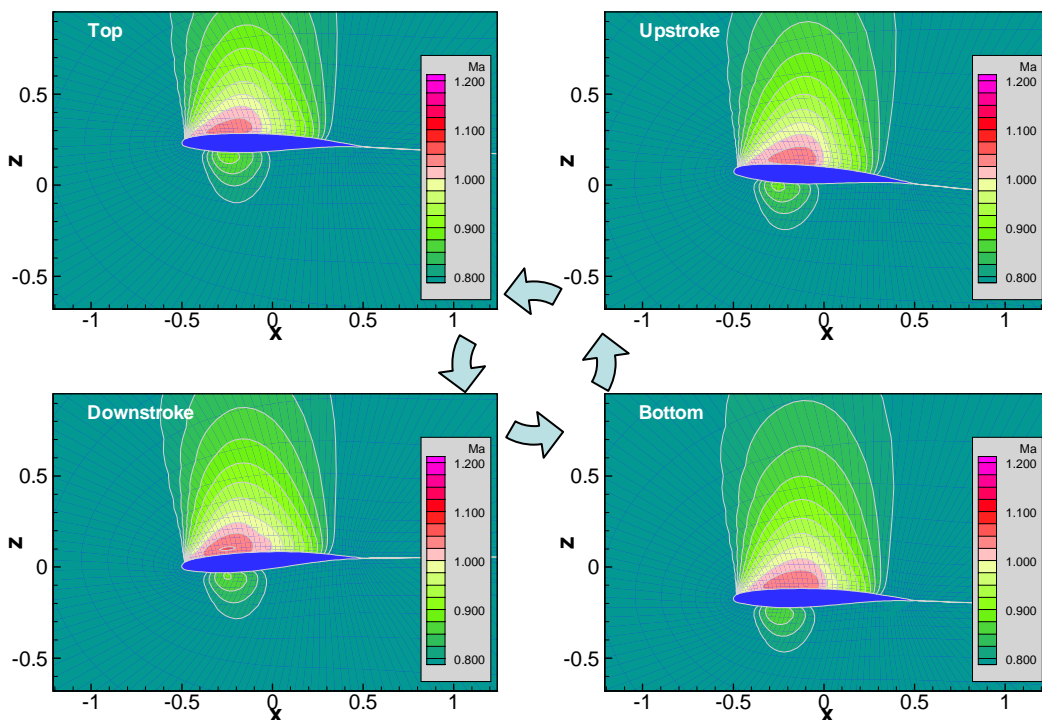


Fig. 5: Mach number around the tip section of a transport aircraft in transonic flow producing thrust. Parameters specified in Fig. 7.

Note the almost unaltered pattern of the contour lines despite the large amplitudes.

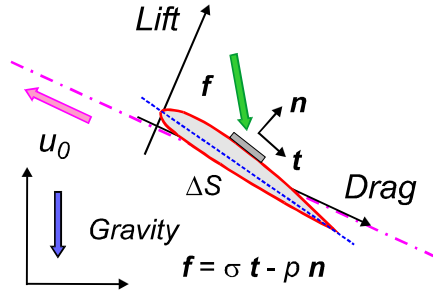


Fig. 6: Lift and drag caused by the fluid force f acting on a surface element ΔS .

0.010394	c_D	6.273E-05	$\langle c_{II,\alpha} \rangle$
0.010038	$\langle c_{II,g} \rangle$	4.222E-04	$\langle c_{II,h} \rangle$
-3.56E-04	Δc_D	4.849E-04	Sum
Drag reduction 3.5 %, Efficiency = 73.45 %			

Tab. 4: Data for Fig. 5.

The power coefficients include α_0^2 .

The difference Δc_D shows the effect of the unsteady motion, which leads to a small drag reduction. The reduction increases for increasing amplitude ratio (Fig. 7) with also improving efficiency, which shows a maximum value for $\lambda_c = 3.9$ close to 90 %. For even larger amplitude ratios the section produces net thrust for one and the same pitch amplitude. Of course, net thrust may also be achieved by simply increasing the pitch amplitude for a fixed amplitude ratio.

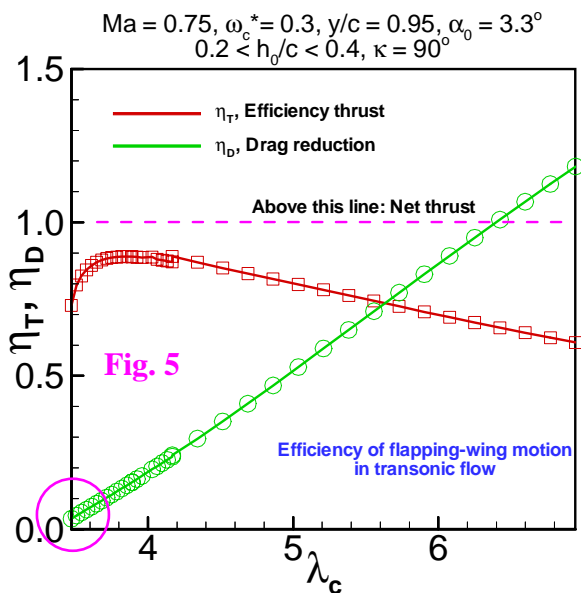


Fig. 7: Wing section transonic transport aircraft

λ_c	$\Delta c_D / \alpha_0^2$	η_T	h_0/c	η_D
3.47	-0.106	0.729	0.200	0.034
3.54	-0.169	0.825	0.204	0.054
3.61	-0.230	0.859	0.208	0.073
3.68	-0.291	0.877	0.212	0.092
3.75	-0.353	0.885	0.216	0.112
3.89	-0.479	0.888	0.224	0.153
3.96	-0.543	0.885	0.228	0.173
<u>4.06</u>	<u>-0.641</u>	<u>0.879</u>	<u>0.234</u>	<u>0.204</u> (I)
4.13	-0.707	0.874	0.238	0.225
4.34	-0.925	0.869	0.250	0.295
4.69	-1.282	0.833	0.270	0.409
<u>5.04</u>	<u>-1.656</u>	<u>0.797</u>	<u>0.290</u>	<u>0.528</u> (II)
5.38	-2.036	0.762	0.310	0.649
5.73	-2.416	0.726	0.330	0.771
6.08	-2.791	0.690	0.350	0.890
6.42	-3.161	0.656	0.370	1.009

Tab. 3: Selected data in Fig. 7.

These values applied, the effect described in the introduction is roughly estimated: At a flight level of 10,000 m, a modern medium size transport aircraft having a weight of 50 tons, a wing area S of 100 m², a span b of 30 m, and a L/D ratio of 18, is assumed to experience the motion in Fig. 5 - for simplicity - with uniform data on 1/5 of its wing area in the tip region. $Ma = 0.75$ leads to a speed over ground of 225 m/s ($q_0 = 1.05 \cdot 10^4$ N/m²) or 810 km/h. The bending motion may be considered the first symmetric bending mode (i.e. $f = 3.2$ Hz, based on $c = S/b$, Reynolds number $2.1 \cdot 10^7$). The acting thrust of 27.25 kN is increased by Δc_D in Tab. 3 using the underlined data in row (I). The additional thrust of 425 N results in 1.75 m/s or about 3.4 knots increase in speed.

Raising the plunge amplitude for fixed λ_c to one chord length gives a pitch amplitude of about 14°. The power produced in this case is 18.3 times higher or 7.8 kN, which is almost 30 % of the total power required. Numerically, full thrust of 27.25 kN with flapping flight is accomplished by amplitudes being eight times larger than in the first case. The plunging amplitude at the tip is about two chord lengths, the pitching amplitude close to 27°, which are quite large values.

The efficiency of 80 % in the second row of the underlined data (II) allows of 1.1 kN

Wing section $y/b = 0.6$, $Ma = 0.75$, $\alpha_s = 0^\circ$, $\omega^* = 0.15 (c/2)$, $\alpha_0 = 3.0^\circ$

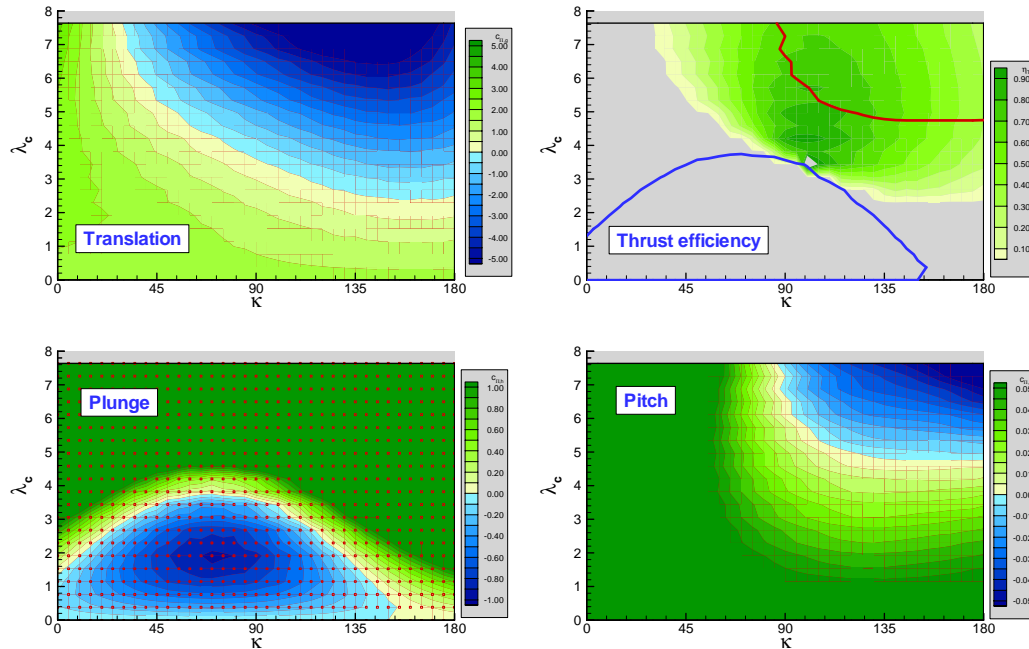
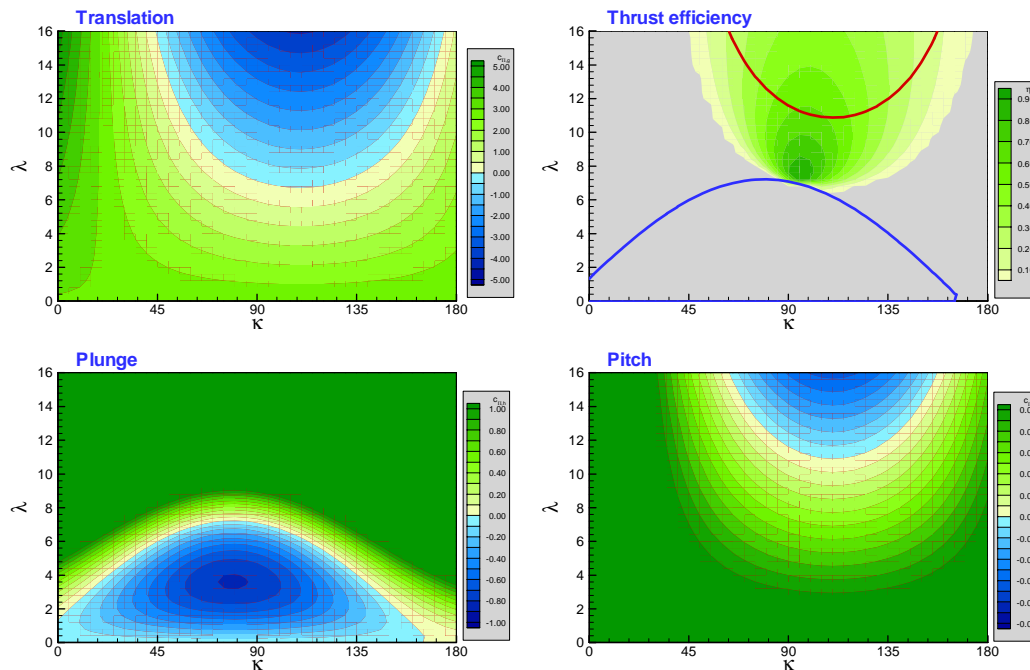


Fig. 9: Wing section of a transonic transport aircraft. Power coefficients from 2D Euler solution compared to the subsonic solution.

The contour lines of level zero for pitch and plunge are copied into the graph for thrust efficiency.

$$(\lambda_c = \lambda/2)$$

2D Thin plate - $Ma = 0.75$, $\alpha_s = 0^\circ$, $\omega^* = 0.15 (c/2)$, $\alpha_0 = 3.0^\circ$



thrust. This value leads to an increase in speed of 4.3 m/s or 8.4 knots.

Full thrust requires $h_0/c = 1.4$ and $\alpha_0 = 16.0^\circ$. It is striking that also for these “large birds” the features of flapping flight remain almost unchanged – at least numerically.

In Fig. 9 the behaviour of the wing section of a transport aircraft is surveyed for various combinations of amplitude ratios and phase shifts. The second left graph displays the individual solutions which were computed. While for the subsonic solutions in Fig. 9 the

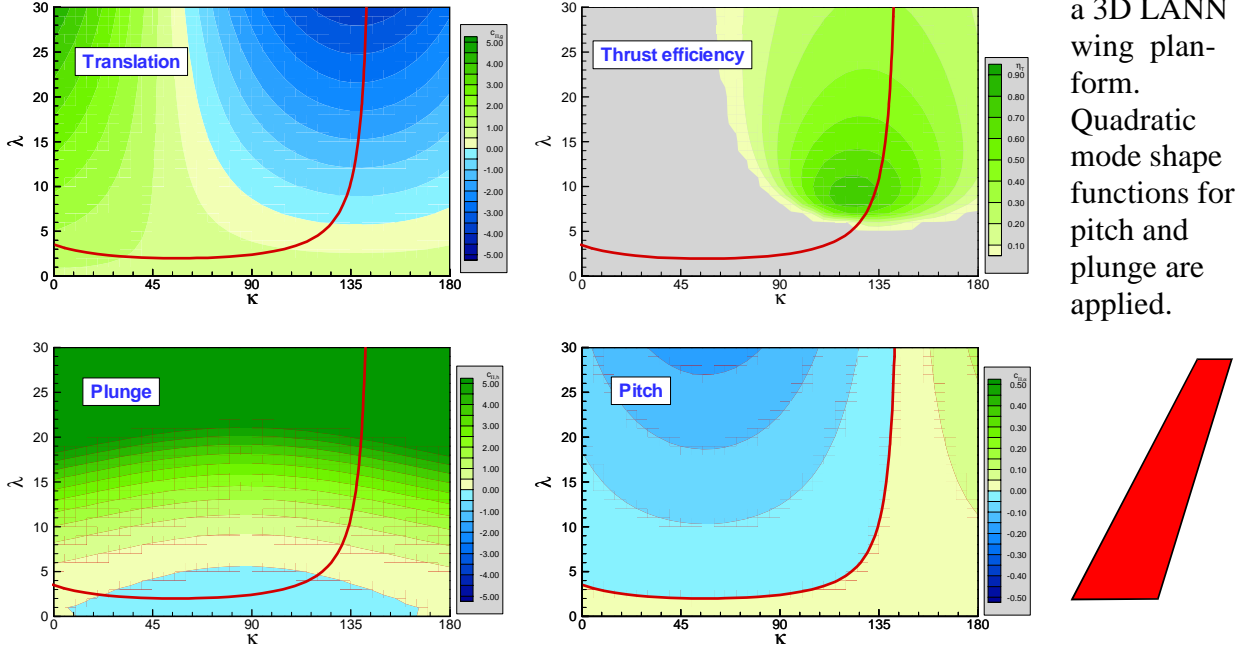
3D Planform - $Ma = 0.0$, $\alpha_s = 0^\circ$, $\omega^* = 0.15 (c/2)$ - LANN Wing, $\phi_T = 27.5^\circ$


Fig. 10: Power coefficients for a 3D LANN wing planform. Quadratic mode shape functions for pitch and plunge are applied.

contributions from pitch and plunge are superimposed, transonic flow requires the full kinematics to be included in each solution. Calculated separately, both the plunging and the pitching motion show strong shocks.

The contour lines of the Euler solution show wiggles and appear to be less accurate than the subsonic plots, which is true. The numerical code requires a “targeted iteration” towards the solution for a specific parameter set (κ, λ) with fixed α_0 . The iteration consists of several periods with values increased step-by-step. The computational time for the overview in Fig. 9 was significantly reduced by stepping from one set to the next on a fine parameter grid without intermediate iterations.

6 3D Planforms and 3D Solutions

2D investigations are not able to include the spanwise effects of individual shapes for bending and torsional modes. Current computational efforts take aim to include the full kinematics of a 3D flexible wing in viscous, compressible flow. Results are hard to achieve because they require long computing times and depend on uncertainties modelling the physical properties of the flow. Contour charts like the

one in Fig. 9 for viscous flow exceed the present computational capabilities. 3D Euler solutions for flapping-wing kinematics were carefully investigated by Neef [14].

The 3D planform model developed includes the 3D kinematics and 2D results for the respective forces and moments in each strip from the wing root to the tip. The spanwise deformations are given in terms of mode shapes and phase shifts among the contributing modes. The example in Fig. 10 shows that the coefficients may depart considerably from the 2D contour pattern. The swept back wing appears to have the optimum efficiency inside the region of passive pitch excitation.

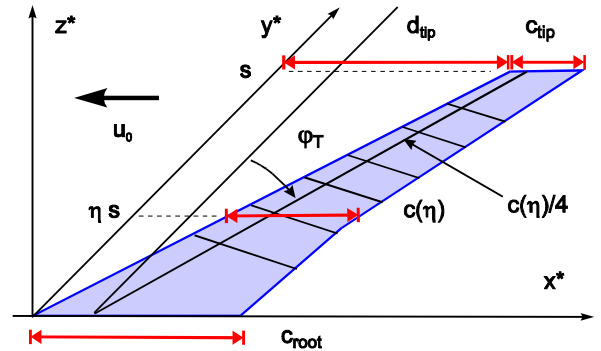


Fig. 11: 3D planform for approximate calculations of 3D kinematics.

7 Perspectives of Technical Use

The most tempting relation considering the technical use of flapping-flight thrust is wing loading over weight in Fig. 12. The path from a design far off the red line (lowest diamond: the Wright Brother's Flyer III) to medium size and large airplanes is enlightening of the evolution of airplanes. The red line may be derived from a theoretical consideration [15] or by interpolating the data.

While human beings never will become "normal" flyers, a modern airplane would well be able to generate sufficient thrust by flapping its wings at a normal rate, provided the technology of actuators exists with the efficiency of modern jet engines – and a wing material enduring thousands of wing beats at large deflections. The probably most useful aspect is the expected reduction of noise for a flying machine which separates the production of the required thrust from the generation of the necessary power (produced in an encapsulated power station), thereby integrating the both functions of carrying weight and producing thrust in the one wing - like flying in nature does. Closer to the near future is the search for potential benefits from *subsidiary* thrust generation, where moderate amplitudes reduce the drag, and the vertically moving trailing edge affects the shedding vortices resulting from the steady lift towards a premature decay. □

References

- [1] Küssner H G. Zusammenfassender Bericht über den instationären Auftrieb von Flügeln, *Luftfahrtforschung* **13**, pp 410-424, 1936.
- [2] Theordorsen Th. General Theory of Aerodynamic Instability and the Mechanism of Flutter, N.A.C.A. Report No. 496, 1935.
- [3] Garrick I E. Propulsion of a Flapping and Oscillating Airfoil, N.A.C.A. Report No. 567, 1936.
- [4] Birnbaum W. Das ebene Problem des schlagenden Flügels, *Zeitschrift für angewandte Mathematik und Mechanik (ZAMM)* **4**, pp 277-292, 1924.
- [5] DeLaurier J D. The Development and Testing of a Full-Scale Piloted Ornithopter, *Canadian Aeronautics and Space J.* Vol. 45, No. 2, pp 72-82, 1999.

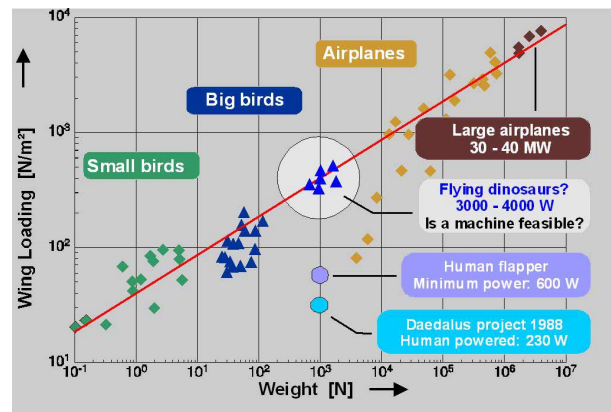


Fig. 12: Wing loading over weight.

- [6] DeLaurier J D. An aerodynamic model for flapping-wing flight, *The Aeronautical Journal* Vol. 97, pp 125-130, April 1993.
- [7] Jones K D, Platzer M F. Numerical computation of Flapping-Wing Propulsion and Power Extraction, 35th Aerospace Sciences Meeting, Jan 6-10, Reno NV, AIAA 97-0826, 1997.
- [8] Jones K D, Dohring C M, Platzer M F. Experimental and Computational Investigation of the Knoller-Betz Effect, *AIAA Journal* Vol. 36. No. 7, pp 1240-1246, 1998.
- [9] Send W. The Mean Power of Forces and Moments in Unsteady Aerodynamics, *Zeitschrift für angewandte Mathematik und Mechanik (ZAMM)* **72**, pp 113-132, 1992.
- [10] Send W. Subsidiäre Schuberzeugung mit gekoppelten Biege- und Torsionsschwingungen in transsonischer Strömung, Deutscher Luft- und Raumfahrtkongress, Sep 27-30, Berlin, DGLR-JT99-086, 1999.
- [11] Carstens V. Berechnung der instationären Druckverteilung an harmonisch schwingenden Gittern in ebener Unterschallströmung, Teil II, DFVLR IB 253-75J02, DFVLR-AVA, Göttingen, 1975.
- [12] Send W. Harmonische Flatteranalyse im Zeitbereich, Deutscher Luft- und Raumfahrtkongress, Nov 17-20, München, DGLR-2003-120, 2003. www.aniprop.de/dglr03
- [13] Carstens V. Computation of the Unsteady Transonic 2D Cascade Flow by an Euler Algorithm with Interactive Grid Generation, AGARD CP 507, Transonic Unsteady Aerodynamics and Aeroelasticity, San Diego, USA, October 7-11, 1991.
- [14] Neef M. Analyse des Schlagfluges durch numerische Strömungsberechnung, PhD Thesis TU Braunschweig, 2002. www.biblio.tu-bs.de.
- [15] Send W. Der Traum vom Fliegen, *Naturwissenschaftliche Rundschau* **56**, Heft 2, pp 65-73, 2003.